1521-009X/50/7/931–941$35.00
DRUG METABOLISM AND DISPOSITION

dx.doi.org/10.1124/dmd.122.000895
Drug Metab Dispos 50:931–941, July 2022

Metabolic Activation of the Acrylamide Michael Acceptor Warhead in Futibatinib to an Epoxide Intermediate Engenders Covalent Inactivation of CYP3A[S]

Lloyd Wei Tat Tang, Jiaxin Fu, Siew Kwan Koh, Guoyi Wu, Lei Zhou, and Eric Chun Yong Chan

Department of Pharmacy, Faculty of Science (L.W.T.T., J.F., G.W., E.C.Y.C.), and Department of Ophthalmology, Yong Loo Lin School of Medicine, National University of Singapore, Singapore (L.Z.); Singapore Eye Research Institute (SERI), Singapore (S.K.K., L.Z.); and Ophthalmology and Visual Sciences Academia Clinical Program, Duke-National University of Singapore Medical School, Singapore (L.Z.)

Received March 14, 2022; accepted April 6, 2022

ABSTRACT

Futibatinib (FUT) is a potent inhibitor of fibroblast growth factor receptor (FGFR) 1–4 that is currently under clinical investigation for intrahepatic cholangiocarcinoma. Unlike its predecessors, FUT possesses an acrylamide warhead, which enables it to bind covalently to a free cysteine residue in the FGFR kinase domain. However, it remains uninterrogated if this electrophilic α,β-unsaturated carbonyl scaffold could also directly or indirectly engender off-target covalent binding to nucleophilic centers on other cellular proteins. Here, we discovered that FUT inactivated both CYP3A isoforms with inactivator concentration at half-maximum inactivation rate constant, maximum inactivation rate constant, and partition ratios of 12.5 and 51.4 μM, 0.25 and 0.06 minutes^{-1}, and ~52 and ~58 for CYP3A4 and CYP3A5, respectively. Along with its time-, concentration-, and cofactor-dependent inhibitory profiles, FUT also exhibited several cardinal features that were consistent with mechanism-based inactivation. Moreover, the nature of inactivation was unlikely to be pseudo-irreversible and instead arose from the covalent modification of the cytochrome P450 apoprotein and/or its heme moiety due to the lack of substantial enzyme activity recovery following dialysis and chemical oxidation, as well as the absence of the diagnostic Soret peak in spectral analyses. Finally, utilizing glutathione (GSH) trapping and high-resolution mass spectrometry, we illuminated that while the acrylamide moiety in FUT could nonenzymatically conjugate to GSH via Michael addition, it was not implicated in the covalent inactivation of CYP3A. Rather, we surmised that it likely stemmed from the metabolic activation of its acrylamide covalent warhead to a highly electrophilic epoxide intermediate that could covalently modify CYP3A and culminate in its catalytic inactivation.

SIGNIFICANCE STATEMENT

In this study, we reported for the first time the inactivation of CYP3A by futibatinib (FUT). Furthermore, using FUT as an exemplary targeted covalent inhibitor, our study revealed the propensity for its acrylamide Michael acceptor moiety to be metabolically activated to a highly electrophilic epoxide. Due to the growing resurgence of covalent inhibitors and the well-established toxicological ramifications associated with epoxides, we advocate that closer scrutiny be adopted when profiling the reactive metabolites of compounds possessing an α,β-unsaturated carbonyl scaffold.

Introduction

Pharmacological repression of fibroblast growth factor receptor (FGFR) signaling pathways is rapidly gaining scientific and therapeutic interest in cancer research (Porta et al., 2017). The impetus for this nascent treatment paradigm was ignited by a landmark genomic profiling study that revealed that FGFR genetic aberrations were prevalent in many solid tumors and subsequently corroborated by multiple lines of preclinical and clinical evidence that validated their oncogenic potential in independently driving tumorigenesis and conferring resistance mechanisms to existing anticancer therapies (Touat et al., 2015; Helsten et al., 2016). Currently, three FGFR-selective inhibitors have already garnered global regulatory approval, with many other promising candidates in advanced stages of clinical development (Chakrabarti et al., 2022). Futibatinib (FUT) (Fig. 1), previously designated as TAS-120, is one such drug that has been accorded Breakthrough Therapy designation by the US Food and Drug Administration (FDA) for the treatment of locally advanced or metastatic intrahepatic cholangiocarcinoma harboring FGFR2-activating mutations (Goyal et al., 2020).

L.W.T.T is supported by the National University of Singapore (NUS) President's Graduate Fellowship (PGF). This work was supported by the Singapore Ministry of Education Tier 1 Academic Research Funding [Grant A-0008501-00-00] (to E.C.Y.C.).

The authors declare that they have no conflicts of interest with the contents of this article.

dx.doi.org/10.1124/dmd.122.000895.

[S] This article has supplemental material available at dmd.aspetjournals.org.

ABBREVIATIONS: DDI, drug-drug interaction; FDA, Food and Drug Administration; FGFR, fibroblast growth factor receptor; FUT, futibatinib; GSH, glutathione; G6P, glucose-6-phosphate; G6PDH, glucose-6-phosphate dehydrogenase; K_I, inactivator concentration at half-maximum inactivation rate constant; k_{inact}, maximum inactivation rate constant; k_{obs}, observed first-order rate constant of inactivation; MBI, mechanism-based inactivation; MIC, metabolite-intermediate complex; NL, neutral loss; P450, cytochrome P450; PIS, precursor ion scan; rhCYP3A4, recombinant human CYP3A4; rhCYP3A5, recombinant human CYP3A5; ROS, reactive oxygen species; $t_{1/2}$, half-life; UPLC-MS/MS, ultra-high performance liquid chromatography tandem mass spectrometry.

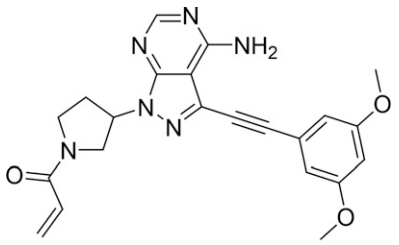

Fig. 1. Chemical structure of futibatinib (FUT).

Preliminary studies by the manufacturer have shown that FUT is chiefly metabolized by CYP3A—the most abundant cytochrome P450 (P450) enzyme isoform expressed in the liver (Yamamiya et al., 2021). Collectively, P450s represent a ubiquitous class of heme-containing enzymes that serve as one of the major drivers of xenobiotic oxidative metabolism in the human body (Guengerich, 2001). In fact, it is widely recognized that the metabolism of around 80% of all drugs marketed to date can be ascribed to just six P450 isoforms (Zanger et al., 2008). However, due to their wide substrate specificities and catalytic promiscuity, P450s may also inadvertently metabolically activate (or bioactivate) drug molecules to electrophilic intermediates (Guengerich, 2011). The chemically reactive species generated may then precipitate immune-mediated idiosyncratic adverse drug reactions when liberated into the cellular milieu due to the wanton and indiscriminate alkylation to nucleophilic centers on biologic macromolecules to form haptens, which may constitute neoantigens that could elicit deleterious autoimmune responses (Masubuchi and Horie, 2007).

One other implication arising from metabolic activation that is germane to drug metabolism and disposition arises from the sequestration of the reactive intermediate within the enzymatic active site by means of covalent adduction to the P450 apoprotein and/or its heme moiety or through complexation with the catalytic ferrous iron (Fe^{2+}), thereby culminating in a distinctive time-dependent loss of its activity via a phenomenon known as mechanism-based inactivation (MBI) (Ho et al., 2015). Unlike direct (or reversible) inhibition of P450s, the loss of catalytic activity evoked by MBI is irreversible, as the covalently modified enzyme is irreparably inactivated and removed from the active pool of P450s. Consequently, the MBI effects continue to persist even after the perpetrator has been systematically eliminated and abated only upon de novo protein synthesis. This explains why the likelihood and severity of drug-drug interactions (DDI) incited by an MBI tend to be more pronounced than with a direct inhibitor (Bjornsson et al., 2003). Apart from its aforementioned time-dependent hallmark, a typical MBI is also known to exhibit these salient features: necessitation of a catalytically competent system (i.e., presence of cofactors), saturable kinetics of inactivation, protection against inactivation by an alternative substrate or competitive inhibitor but not by exogenous nucleophilic scavengers, irreversibility of inactivation, and a 1:1 binding stoichiometry (Silverman, 1995).

Our laboratory has recently established that the three FDA-approved FGFR inhibitors—namely erdafitinib, pemigatinib, and infigratinib—elicited MBI of CYP3A (Tang et al., 2021a,b; Tang et al., 2022). We also deciphered the underlying metabolic activation pathways leading to the formation of the electrophilic intermediates implicated in the covalent modification of the P450 apoprotein. Unlike its predecessors, FUT is a targeted covalent inhibitor that possesses an electrophilic acrylamide warhead, which enables it to covalently bind to a unique free cysteine residue in the FGFR kinase domain (Sootome et al., 2020). Although this has allowed it to elude drug resistance associated with conventional reversible ATP-competitive FGFR inhibitors, it may also increase its predisposition to cause off-target covalent binding. This factor, along with a previous report that revealed that FUT also inhibited CYP3A in vitro (Yamamiya et al., 2021), led us to posit that FUT is metabolically activated to a reactive intermediate that engenders covalent inactivation of CYP3A.

In this study, we reported for the first time that FUT inactivates CYP3A4 and CYP3A5 in a time-, concentration-, and cofactor-dependent manner consistent with MBI. Subsequently, glutathione (GSH) trapping experiments and high-resolution mass spectrometry revealed that FUT undergoes P450-mediated metabolic activation at its acrylamide Michael acceptor warhead to an epoxide intermediate which covalently inactivates CYP3A.

Materials and Methods

Chemicals and Reagents. Erdafitinib and FUT were purchased from MedChem Express (Monmouth Junction, NJ). Catalase, dexamethasone, GSH, ketoconazole, and rivaroxaban were procured from Sigma-Aldrich (St. Louis, MO). Potassium ferricyanide was acquired from VWR International (Leuven, Belgium). Recombinant human CYP3A4 (rhCYP3A4) and CYP3A5 (rhCYP3A5) Supersomes coexpressing both NADPH P450 oxidoreductase and cytochrome b_5 and the NADPH-regenerating system comprising NADP+ and glucose-6-phosphate (G6P) and glucose-6-phosphate dehydrogenase (G6PDH) were commercially purchased from Corning Gentest (Woburn, MA). High-performance liquid chromatography–grade acetonitrile was procured from Tedia Company Inc. (Fairfield, OH). Ultrapure water (type I) was prepared in our laboratory using a Milli-Q water purification system (Millipore Corporation, Bedford, MA).

Substrate Depletion of FUT by CYP3A. Triplicate incubation mixtures comprising 20 pmol/mL rhCYP3A4/5, FUT (1 μM), G6PDH, and potassium phosphate buffer (100 mM; pH 7.4) were prepared and prewarmed at 37°C for 5 minutes. The following reaction was initiated via the addition of NADP+/G6P (final NADPH concentration 1 mM). At each predefined time interval (0, 5, 10, 15, 30, 45, 60, 80, 100, and 120 minutes), aliquots of each incubation mixture were withdrawn and added to an equal volume of ice-cold acetonitrile spiked with internal standard (0.1 μM erdafitinib) to stop the reaction. The quenched samples were then centrifuged at 4000*g* at 4°C for 30 minutes, after which the supernatant was withdrawn and analyzed by ultrahigh-performance liquid chromatography-tandem mass spectrometry (UPLC-MS/MS) to quantify the amount of FUT remaining as previously described (Tang and Chan, 2022).

Time-, Concentration-, and NADPH-Dependent Inactivation of CYP3A. CYP3A inactivation kinetic assays were performed as described in our recent works using the factor X_a direct anticoagulant rivaroxaban as a clinically sensitive probe substrate of CYP3A (Tang et al., 2021a,b; Tang et al., 2022). Briefly, triplicate primary incubation mixtures comprising 40 pmol/mL rhCYP3A4/5, FUT (i.e., 0–25 μM for CYP3A4 incubations and 0–50 μM for CYP3A5 incubations), G6PDH and potassium phosphate buffer (100 mM; pH 7.4) were prepared and prewarmed at 37°C for 5 minutes. Thereafter, the reaction was initiated via the addition of NADP+/G6P. Subsequently, at various preincubation intervals (i.e., 0, 3, 6, 9, 12, and 15 minutes), aliquots of each primary incubation mixture were withdrawn and diluted 20-fold into a prewarmed secondary incubation mixture which consisted of saturating concentrations of rivaroxaban (50 μM; concentration corresponding to ~4× Michaelis constant), an NADPH- regenerating system (1 mM), and potassium phosphate buffer (100 mM; pH 7.4). The secondary incubation mixtures were then further incubated for 2 hours at 37°C. Then aliquots of the secondary incubation mixture were immediately withdrawn and added to an equal volume of ice-cold acetonitrile spiked with internal standard (4 μM dexamethasone). The quenched samples were then centrifuged at 4000*g* at 4°C for 30 minutes to obtain the supernatant for UPLC-MS/MS quantification of hydroxylated rivaroxaban, which served as a surrogate for the amount of CYP3A activity remaining (Supplemental Methods; Supplemental Table 1). Negative control experiments were performed by replacing NADP+/G6P with potassium phosphate buffer (100 mM; pH 7.4).

Calculation of MBI Kinetic Parameters. To derive the inactivator concentration at half-maximum inactivation rate constant (K_I) and maximum

inactivation rate constant (k_{inact}), the means of triplicate peak area ratios were used to calculate the natural logarithm of percentage P450 enzyme activity remaining normalized to vehicle, which was then subsequently plotted against preincubation time for each FUT concentration. The resulting data points were fitted to linear regression and the observed first-order inactivation rate constant (k_{obs}) of FUT against CYP3A-mediated rivaroxaban hydroxylation was estimated from the slope of the initial linear decline in CYP3A activity for each FUT concentration. Specifically, points from preincubation timepoints 0 to 12 minutes were adopted in the calculation of the k_{obs} in CYP3A4 incubations due to a loss of linearity occurring at 15-minute timepoint. Conversely, in CYP3A5 incubations, points throughout 0 to 15 minutes were used, as the decline in enzymatic activity was determined to be linear throughout. After which, a plot of k_{obs} against FUT concentrations [I] allowed the fitting of inactivation kinetic constants (K_I and k_{inact}) to nonlinear least square regression based on Eq. 1 in GraphPad 8.0.2 (San Diego, CA):

$$k_{obs} = \frac{k_{inact} \times [I]}{K_I + [I]}. \quad (1)$$

Eq. 1 assumes that the change of [I] during the preincubation period is negligible and that the loss of enzymatic activity purely stems from inactivation by FUT. Moreover, it was also assumed that the nonspecific binding of FUT to rhCYP3A4/5 in the preincubation mixtures was minimal, thus the apparent K_I values described in this work were derived from total drug concentrations rather than unbound drug concentrations. The k_{inact}/K_I ratio was determined by dividing the mean values of k_{inact} by K_I. Lastly, the time required for half of the enzyme molecules to be inactivated ($t_{1/2}$) was determined by Eq. 2:

$$t_{1/2} = \frac{ln2}{k_{inact}}. \quad (2)$$

Partition Ratio. Triplicate primary incubation mixtures consisting of 100 pmol/mL rhCYP3A4/5, FUT (0, 1, 2.5, 5, 15, 25, and 50 μM), G6PDH, and potassium phosphate buffer (100 mM; pH 7.4) were prepared and prewarmed at 37°C for 5 minutes, and the reaction was subsequently initiated via the addition of NADP+/G6P. The reaction mixtures were incubated for a protracted duration of 45 minutes to allow CYP3A inactivation by FUT to go into completion. Thereafter, aliquots of the primary incubation mixture were withdrawn and diluted 20-fold into the prewarmed secondary incubation mixture (similar to that prepared for the aforementioned inactivation assays) and incubated at 37°C for a further 2 hours. Samples were then quenched, centrifuged, and assayed for residual CYP3A enzyme activity by UPLC-MS/MS (Supplemental Methods). The turnover number and partition ratio was computed as outlined in our previous study (Tang et al., 2021c). Briefly, the percentage of residual CYP3A activity was plotted against the molar ratio of FUT to CYP3A concentration (i.e., 0–500). The turnover number was computed by determining the intercept of the straight line plotted at lower molar ratios with the linear regression line plotted at higher molar ratios to the abscissa. Finally, the partition ratio was back calculated by subtracting the turnover number by a numerical value of 1.

Substrate Protection. To investigate if enzyme inactivation was amenable to substrate protection, an alternative CYP3A substrate (testosterone) or a potent direct inhibitor of CYP3A (ketoconazole) was individually introduced into the reaction mixtures. Triplicate primary incubation comprising 40 pmol/mL rhCYP3A4/5, FUT (25 μM), G6PDH, potassium phosphate buffer (100 mM; pH 7.4), and either testosterone (100 and 200 μM; equivalent to 1:4 and 1:8 molar ratio of FUT:testosterone) or ketoconazole (0.1 and 1 μM; corresponding to ~1× and ~10× its K_i value) were prepared. The reaction was initiated via the addition of NADP+/G6P after prewarming at 37°C for 5 minutes. Aliquots were withdrawn at different preincubation time points (i.e., 0, 3, 6, and 9 minutes for CYP3A4 incubations and 0, 6, 12, and 15 minutes for CYP3A5 incubations), transferred to the secondary incubation mixture and subsequently quenched, centrifuged and assayed for residual CYP3A enzymatic activity by UPLC-MS/MS (Supplemental Methods). Primary incubation mixtures that omitted the addition of either testosterone, ketoconazole, or both FUT and testosterone or ketoconazole served as the negative controls.

Effect of Exogenous Nucleophile and Scavenger of Reactive Oxygen Species on Inactivation. Triplicate primary incubation mixture containing 40 pmol/mL rhCYP3A4/5, FUT (25 μM), G6PDH, and potassium phosphate buffer (100 mM; pH 7.4) were individually enriched with either GSH (2 mM) or catalase (800 U/mL), which were employed as an exogenous nucleophile and scavenger of reactive oxygen species (ROS), respectively. After prewarming at 37°C for 5 minutes, the enzymatic reaction was initiated via the addition of NADP+/G6P. At specific preincubation time points (i.e., 0, 3, 6, and 9 minutes for CYP3A4 incubations and 0, 6, 12, and 15 minutes for CYP3A5 incubations), aliquots were transferred to the secondary incubation mixtures and subsequently quenched, centrifuged and assayed for residual CYP3A enzymatic activity by UPLC-MS/MS (Supplemental Methods). Primary incubation mixtures that obviated the addition of either GSH or catalase or both FUT and GSH or catalase served as the negative controls.

Reversibility of Inactivation. The reversibility of CYP3A inactivation was evaluated by two complementary methodologies; namely dialysis and chemical oxidation by potassium ferricyanide, as described in greater detail in our previous works (Tang et al., 2021b; Tang et al., 2022). In the first series of experiments involving dialysis, triplicate primary incubation mixtures comprising 40 pmol/mL rhCYP3A4/5, FUT (0 or 25 μM), G6PDH, and potassium phosphate buffer (100 mM; pH 7.4) were preincubated at 37°C for 5 minutes. Enzymatic reaction was initiated by the addition of NADP+/G6P and allowed to proceed for 30 minutes. Then a 5 μL aliquot was transferred to the secondary incubation mixture yielding a 20-fold dilution. Concurrently, the remaining primary incubation mixture (approximately 90 μL) was transferred to a Slide-A-Lyzer MINI Dialysis Device (molecular weight cutoff of 10,000 Da; Pierce Chemical Co., Rockford, IL) and gently lowered into a glass beaker filled with 500 mL of ice-cold potassium phosphate buffer (100 mM; pH 7.4). The buffer system was maintained on ice (4°C) with constant gentle stirring and accompanied by one fresh buffer change at the second hour mark. After 4 hours, a 5 μL aliquot of the dialyzed mixture was transferred to each prewarmed secondary incubation well. All secondary mixtures were further incubated at 37°C for 2 hours and subsequently assayed for residual CYP3A enzymatic activity by UPLC-MS/MS (Supplemental Methods).

In the second series of experiments involving chemical oxidation with potassium ferricyanide, three sequential incubations were performed. Briefly, the primary incubation consisted of 40 pmol/mL rhCYP3A4/5, FUT (0 or 25 μM), G6PDH, and potassium phosphate buffer (100 mM; pH 7.4). Following the initiation of the reaction with the addition of NADP+/G6P and incubation at 37°C for either 0 or 30 minutes, 20 μL of the primary incubation mixture was aliquoted into an equal volume of secondary incubation mixture containing potassium phosphate buffer (100 mM; pH 7.4) with or without potassium ferricyanide (2 mM). The secondary mixtures were then allowed to incubate at 37°C for another 10 minutes. Thereafter, 10 μL of the mixture was withdrawn and diluted 10-fold into a tertiary incubation mixture containing rivaroxaban (50 μM), an NADPH-regenerating system (1 mM), and potassium phosphate buffer (100 mM; pH 7.4). The reaction mixture was further incubated at 37°C for another 2 hours and subsequently assayed for residual CYP3A activity by UPLC-MS/MS (Supplemental Methods). The percentage of CYP3A metabolic activity remaining after 0 or 30 minutes incubation with FUT compared with the corresponding controls in the absence of FUT was calculated using Eq. 3 and 4 respectively.

$$\%\ \text{control}_{0\ min} = \frac{v_{(0\text{min},(+)\ FUT)}}{v_{(0\text{min},(-)\ FUT)}} \times 100 \quad (3)$$

$$\%\ \text{control}_{30\ min} = \frac{v_{(30\text{min},(+)\ FUT)}}{v_{(30\text{min},(-)\ FUT)}} \times 100 \quad (4)$$

where v represents the residual CYP3A activity. Thereafter, percentage of restoration of metabolic activity of CYP3A was derived by subtracting % $\text{control}_{30\ min}$ in the presence of potassium ferricyanide from the corresponding values obtained in the absence of potassium ferricyanide.

Spectral Difference Scanning. Incubation mixtures containing 200 pmol/mL rhCYP3A4/5, FUT (25 μM), G6PDH and potassium phosphate buffer (100 mM; pH 7.4) were prepared, prewarmed at 37°C for 5 minutes, and initiated via the addition of NADP+/G6P. At the same time, they were immediately scanned from 400 to 500 nm at 5-minute intervals over 1 hour using a Hidex Sense microplate reader (Hidex, Turku, Finland) at 37°C. The spectral differences were obtained by comparing the UV absorbances between the sample and reference wells, which consisted of vehicle in place of FUT. Additionally, the degree of metabolite-intermediate complex (MIC) formation was also semiquantitatively assessed by measuring the absorbance difference between 454 and 490 nm with time.

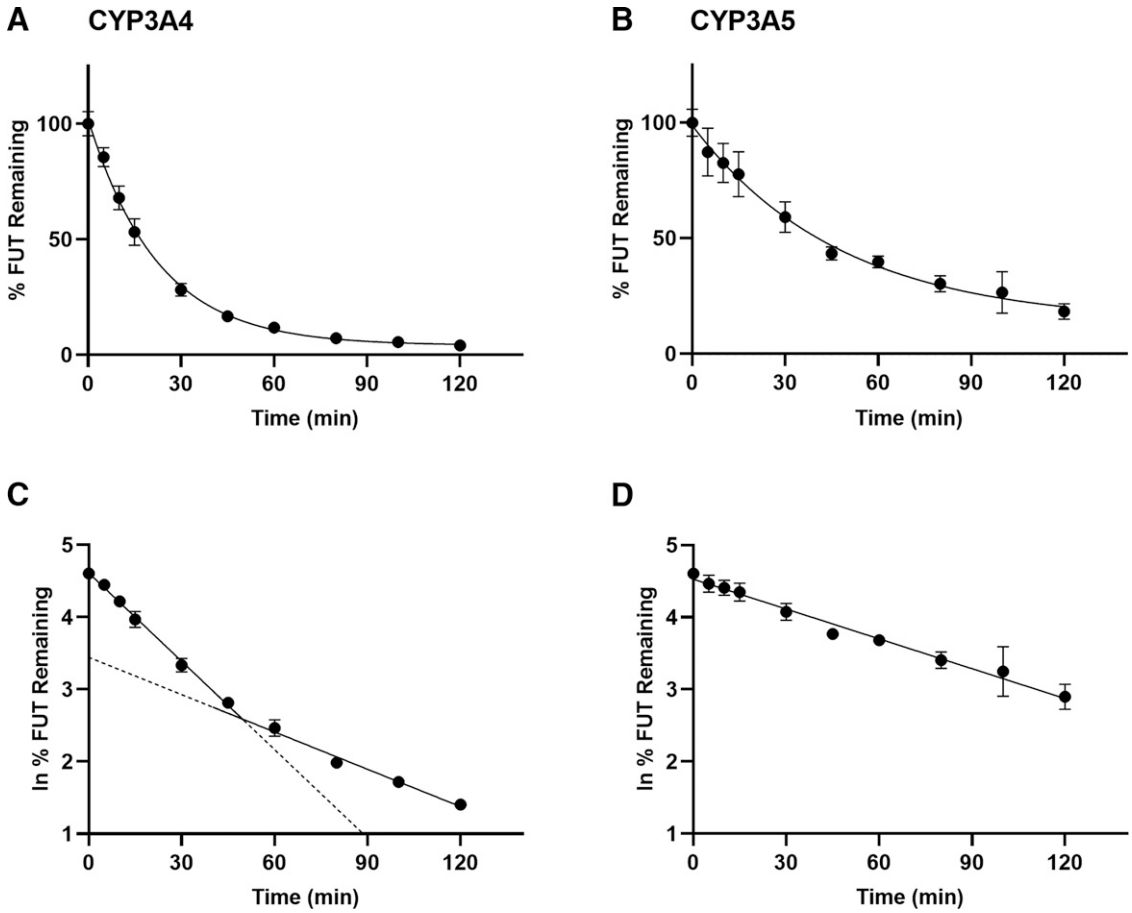

Fig. 2. Substrate depletion of FUT by CYP3A. Percentage of FUT remaining against time in the presence of (A) CYP3A4 and (B) CYP3A5 plotted on a linear scale and the corresponding substrate depletion graphs of FUT in (C) CYP3A4 and (D) CYP3A5 as plotted on a semilog scale. Each point in A–D represents the mean and S.D. of triplicate experiments.

GSH Trapping Assay. GSH trapping experiments were performed as previously described with minor modifications (Tang et al., 2021a,b). Incubation mixtures containing 50 pmol/mL rhCYP3A4, FUT (25 μM), G6PDH, and potassium phosphate buffer (100 mM; pH 7.4) were fortified with GSH (50 mM) and prewarmed at 37°C for 5 minutes. The reaction was then initiated via the addition of NADP+/G6P and incubated at 37°C for 1 hour. After which, an equal volume of ice-cold acetonitrile was added to quench the reaction. The resulting mixture was centrifuged at 14,000*g* at 4°C for 15 minutes. Then the supernatant was transferred to a new microcentrifuge tube and concentrated using a gentle stream of nitrogen gas (TurboVap LV; Caliper Life Science, Hopkinton, MA). The residue was subsequently reconstituted with 60 μL of acetonitrile-water mixture (3:7), vortexed and centrifuged at 14,000*g* at 4°C for 15 minutes. The resulting supernatant was then carefully removed and transferred to a fresh vial to detect FUT-derived GSH adducts via UPLC-MS/MS. Samples that omitted the inclusion of FUT or rhCYP3A4 in the incubation mixture served as the vehicle and enzyme-free controls, respectively.

Detection of GSH Adducts by UPLC-MS/MS. GSH adducts of FUT formed in situ in the GSH trapping assay were detected using the UPLC-MS/MS system comprising an Agilent 1290 Infinity ultrahigh-pressure liquid chromatography (Agilent Technologies Inc., Santa Clara, CA) interfaced with a triple quadrupole linear ion trap mass spectrometer (AB SCIEX QTRAP 5500 MS system equipped with a Turbo V ion source; AB SCIEX, Framingham, MA). Chromatographic separation was achieved on an ACQUITY UPLC ethylene bridged hybrid C_{18}, 2.2 × 100 mm, 1.7 μM column (Waters, Milford, MA) using 0.1%

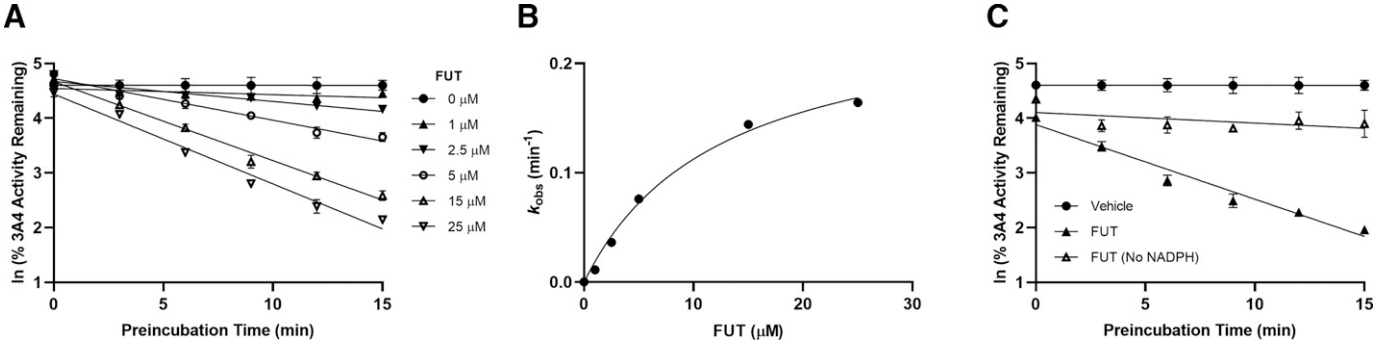

Fig. 3. (A) Time- and concentration-dependent inactivation of CYP3A4-mediated rivaroxaban hydroxylation by FUT. (B) Nonlinear least square regression of k_{obs} versus various concentrations of FUT yielded K_I and k_{inact} values of 12.5 ± 2.4 μM and 0.25 ± 0.02 minutes^{-1}. (C) Inactivation of CYP3A4 by FUT also exhibited cofactor-dependency. Each point in A–C represents the mean and S.D. of triplicate experiments.

TABLE 1

CYP3A4 and CYP3A5 inactivation kinetic parameters for FUT derived using morpholinone hydroxylation of rivaroxaban as an in vitro marker reaction of residual CYP3A activity

Data are presented as means ± S.D.

P450 Isoform	K_I (μM)	k_{inact} (min^{-1})	k_{inact}/K_I ($min^{-1}mM^{-1}$)	$t_{1/2}$ (min)	Partition Ratio
CYP3A4	12.5 ± 2.4	0.25 ± 0.02	20.0	2.8	52
CYP3A5	51.4 ± 21.4	0.06 ± 0.02	1.2	11.6	58

formic acid in water (A) and 0.1% formic acid in acetonitrile as the mobile phases. Mobile phases were delivered at a flow rate of 0.35 mL/min. The column and sample temperature were set at 45°C and 4°C respectively. The gradient elution conditions were as follows: isocratic at 10% B (0–2.00 minutes), linear gradient 10%–70% B (2.01–12.00 minutes), linear gradient 70%–90% B (12.01–14.00 minutes), isocratic at 90% B (14.01–18.00 minutes), isocratic at 10% B (18.01–20.00 minutes). An information-dependent acquisition experiment was conducted to detect FUT-derived GSH conjugates using two well-established survey scans—namely, a precursor ion scan (PIS) of *m/z* 272 in negative ESI mode and a constant neutral loss (NL) scan of 129 Da in positive electrospray ionization (ESI) mode. An enhanced product ion scan was subsequently performed for all putative GSH adducts identified in positive ESI mode. The source-dependent mass spectrometry parameters used were as follows: ion spray voltage: 4500 V; source temperature: 500°C; curtain gas: 30 psi; ion source gas 1 (sheath gas): 50 psi; ion source gas 2 (drying gas): 50 psi.

The accurate masses of the GSH adducts prospectively identified by the aforementioned QTRAP-MS were then measured using an ACQUITY ultrahigh-pressure liquid chromatography (Waters, Milford, MA) coupled with an Orbitrap Exploris 480 MS (Thermo Fisher Scientific, San Jose, CA). The C_{18} column, mobile phases, flow rate, temperature, and gradient elution conditions were identical to those described earlier in this section. The injection volume was 3 μL and the analytes were ionized by ESI in positive ion mode under the following conditions: sheath gas: 50 arbitrary units; auxiliary gas: 10 arbitrary units; sweep gas: 1 arbitrary unit; S-lens: 50; ion transfer tube temperature: 325°C; vaporizer temperature: 350°C. A normalized collision energy of 20% was applied to fragment all ions. The Orbitrap-MS data were acquired and further processed using Xcalibur 4.4 and Freestyle 1.7 software (Thermo Fisher Scientific, San Jose, CA).

Results

Substrate Depletion of FUT in CYP3A. While FUT was previously reported to inhibit CYP3A in vitro (Yamamiya et al., 2021), the

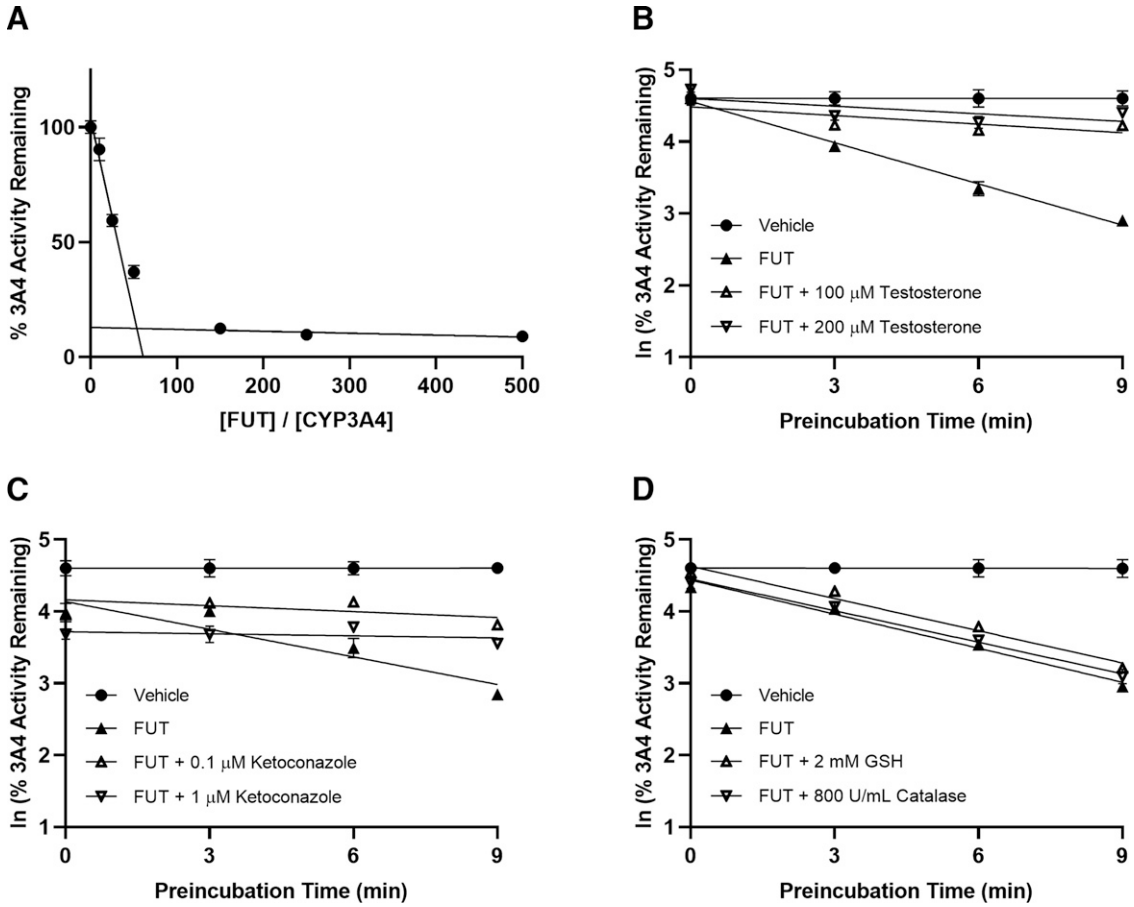

Fig. 4. (A) Partition ratio for the inactivation of CYP3A4 by FUT was estimated to be 52, implying that enzyme inactivation was efficient. Inactivation of CYP3A4 was diminished by coincubation with (B) an alternative CYP3A substrate (testosterone) and considerably abrogated by (C) a direct inhibitor of CYP3A (ketoconazole). (D) The inclusion of either an exogenous nucleophile (GSH) or a scavenger of ROS (catalase) did not confer substrate protection. Each point in A–D represents the mean and S.D. of triplicate experiments.

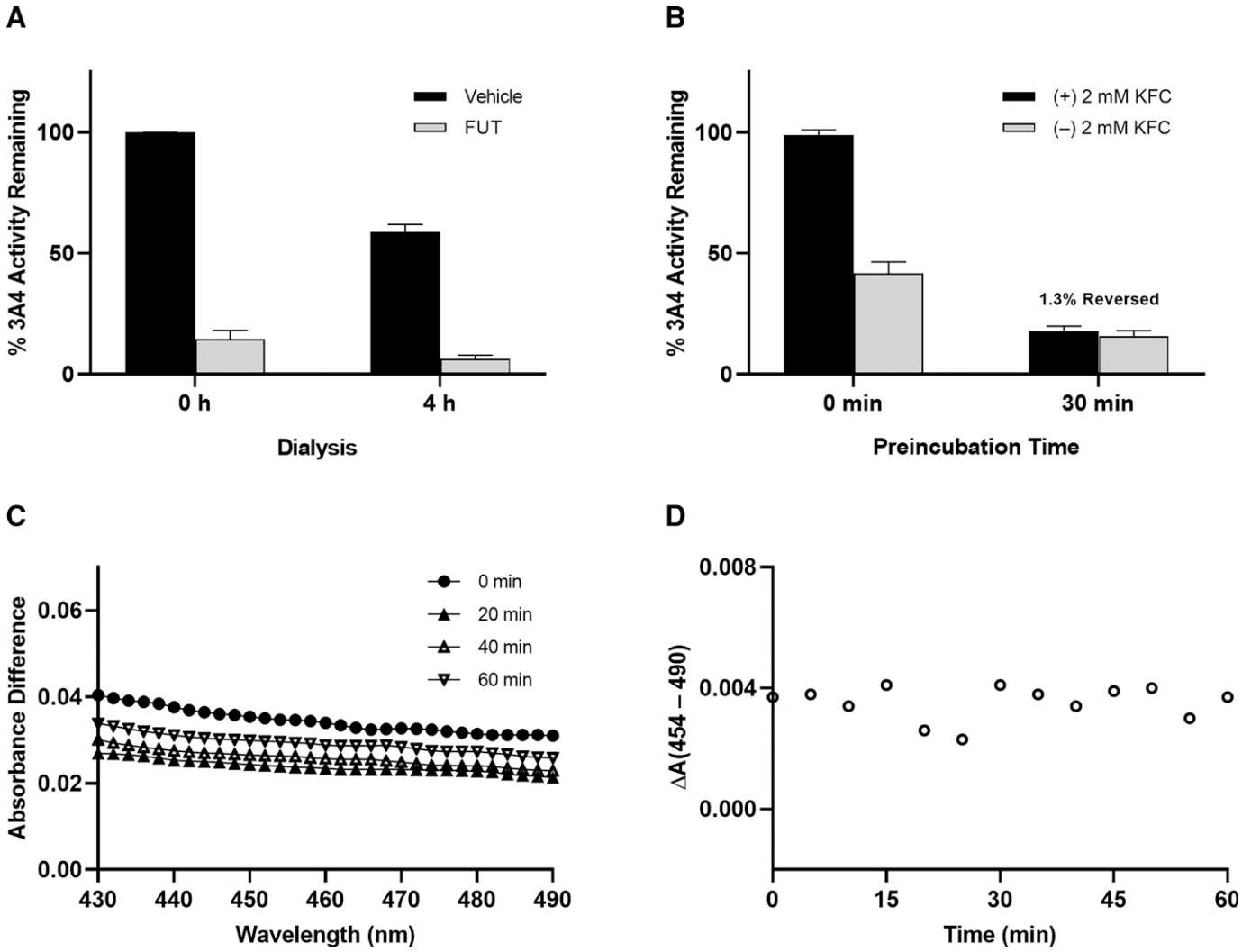

Fig. 5. Metabolic activity of CYP3A4 was (A) not restored after extensive dialysis at 4°C for 4 hours and (B) only modestly restored by 1.3 ± 0.3% following treatment with 2 mM potassium ferricyanide (KFC). (C) Absorbance difference measured over 1 hour failed to detect a spectrally resolvable peak in the Soret region (448–458 nm) for CYP3A4 incubated with FUT. (D) Likewise, a comparison of the absorbance at the reference of 454 nm against the isosbestic point at 490 nm failed to demonstrate an increase in the extent of MIC formation over time. Results from A and B depict the mean and S.D. of three independent experiments conducted in triplicates.

exact biochemical nature underscoring its inhibition remains obscure. Consequently, to evaluate if FUT elicits any considerable time-dependent inhibition of CYP3A, we first monitored the depletion of 1 μM FUT in rhCYP3A4/5 over a period of 2 hours. Our findings corroborated earlier reports by the manufacturer that FUT is predominantly metabolized by CYP3A, due to the rapid turnover of FUT observed in our substrate depletion assay (Yamamiya et al., 2021). Notably, FUT appeared to be metabolized more efficiently by CYP3A4, with 11.8 ± 1.4% of the parent drug remaining after a 1-hour incubation with rhCYP3A4 (Fig. 2A), as compared with 39.8 ± 2.5% in rhCYP3A5 incubations (Fig. 2B). Applying a log transformation gave rise to two distinct linear phases in the substrate depletion profile of FUT in CYP3A4 (Fig. 2C), whereas a single linear phase was observed for that of CYP3A5 (Fig. 2D). Consequently, two different elimination rate constants (termed $k_{fast,3A4}$ and $k_{slow,3A4}$) were calculated for CYP3A4. Juxtaposing the elimination rate constant for CYP3A4 obtained in the initial portion of incubation with that of CYP3A5 revealed that FUT was metabolized ~3× faster by CYP3A4 as compared with CYP3A5 (i.e., $k_{fast,3A4}$ = 0.041 ± 0.001 minute^{-1} compared with k_{3A5} = 0.014 ± 0.001 minutes^{-1}). However, after about 1 hour, there was a marked reduction in the elimination rate constant of FUT by CYP3A4 (i.e., $k_{slow,3A4}$ = 0.017 ± 0.001 minutes^{-1}), which seems to suggest that either significant loss of the substrate has occurred or that time-dependent inhibition (or inactivation) of the enzyme had taken place.

Time-, Concentration-, and Cofactor-Dependent Inactivation of CYP3A by FUT. We then proceeded to quantitatively investigate its inactivation kinetics using rivaroxaban, a clinically sensitive probe of CYP3A. Our findings confirmed that FUT inactivated CYP3A4-mediated rivaroxaban hydroxylation in a time- and concentration-dependent manner (Fig. 3A), with the greatest loss of rivaroxaban hydroxylase activity attained when 25 μM FUT was preincubated for 15 minutes with CYP3A4. Moreover, as the k_{obs} of FUT against CYP3A4 tended toward a maximum rate (i.e., k_{inact}) (Fig. 3B), it denoted that the loss of CYP3A4 activity elicited by FUT is saturable and exhibited pseudo–first-order kinetics. The K_I and k_{inact} of FUT derived from the Kitz-Wilson plot (Kitz and Wilson, 1962) were determined to be 12.5 ± 2.4 μM and 0.25 ± 0.02 minutes^{-1} respectively, which in turn yielded a k_{inact}/K_I ratio of 20.0 minutes^{-1}mM^{-1} and inactivation $t_{1/2}$ of 2.8 minutes. Furthermore, the exclusion of NADPH—which serves as an important cofactor in P450-mediated metabolic reactions—completely nullified the

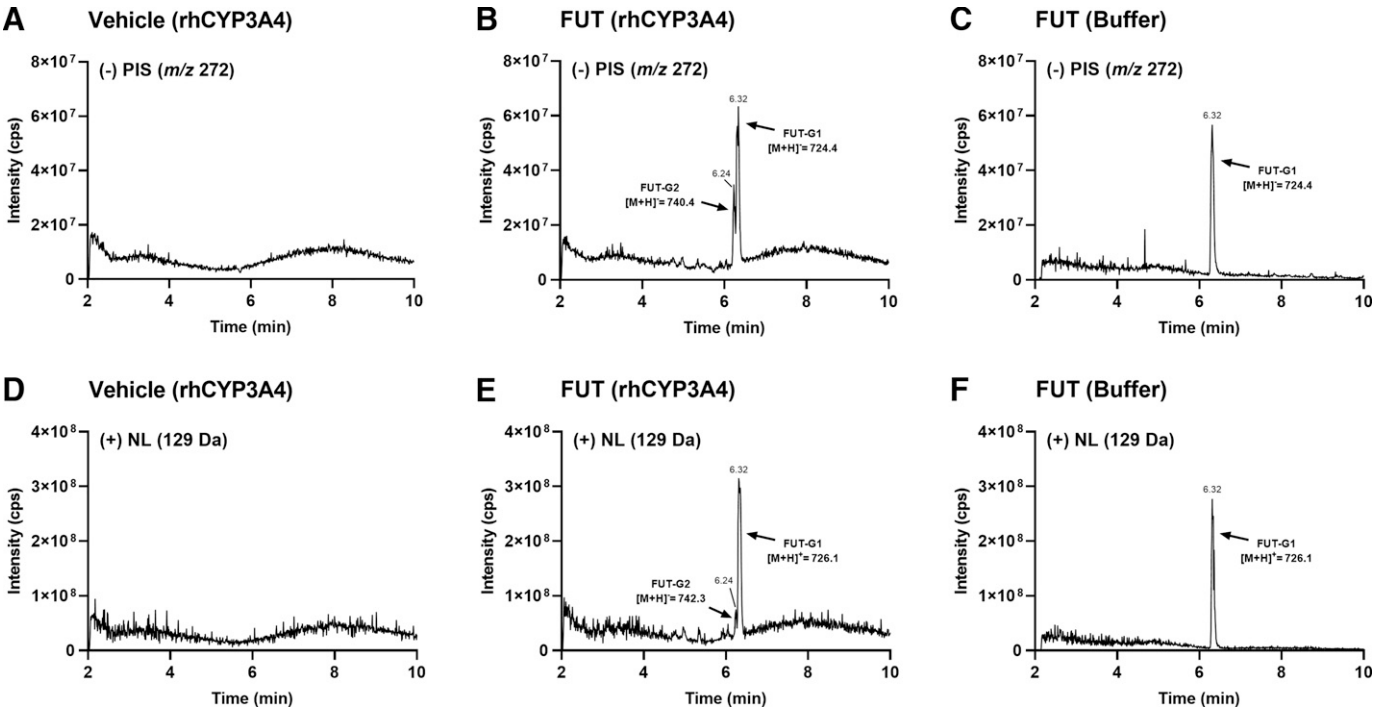

Fig. 6. Total ion chromatogram for PIS of *m/z* 272 in negative ESI mode of (A) vehicle, (B) FUT (rhCYP3A4), and (C) FUT buffer (enzyme-free) incubation mixtures fortified with 50 mM GSH. Total ion chromatogram for constant NL scan of 129 Da in positive ESI mode of the same aforementioned (D) vehicle, (E) FUT (rhCYP3A4), and (F) FUT buffer (enzyme-free) incubation mixtures. Notably, while a peak corresponding to the FUT-derived GSH adduct FUT-G1 (retention time: 6.32 minutes) was detected in both survey scans for incubation mixture comprising FUT, an additional but less abundant GSH adduct FUT-G2 (retention time: 6.24 minute) was present only in FUT incubation mixtures that contained rhCYP3A4 and absent in FUT buffer incubation mixtures.

loss of CYP3A4-mediated rivaroxaban hydroxylase activity by FUT (Fig. 3C). Therefore, metabolic activation of FUT is an instrumental preceding molecular event that is necessary for enzyme inactivation. Unexpectedly, parallel experiments with CYP3A5 also revealed that FUT elicited time-, concentration-, and cofactor-dependent inactivation of CYP3A5-mediated rivaroxaban hydroxylation with K_I and k_{inact} values of 51.4 ± 21.4 μM and 0.06 ± 0.02 minutes^{-1}, respectively (Supplemental Fig. 1, A–C). This in turn translated to a k_{inact}/K_I ratio of 1.2 minutes^{-1}mM^{-1} and an inactivation $t_{1/2}$ of 11.6 minutes. Taken together, our results revealed that the inactivation of CYP3A5 by FUT was ∼16.7× less potent than that of CYP3A4, which could explain why the earlier substrate depletion plot for CYP3A5 did not exhibit a biphasic profile akin to that of CYP3A4. All values of K_I, k_{inact}, k_{inact}/K_I ratio, and $t_{1/2}$ reported in this work are summarized in Table 1.

Partition Ratio. The partition ratio is an estimate of the number of inactivator molecules that are metabolized and liberated from the enzymatic site without causing inactivation relative to each molecule of the enzyme that gets inactivated (Orr et al., 2012). Adopting a previously described titration method (Silverman, 1995), the turnover numbers for the inactivation of CYP3A4 and CYP3A5 by FUT were found to be ∼53 and ∼59, respectively (Fig. 4A) (Supplemental Fig. 2A). This in turn corresponded to a partition ratio of ∼52 for CYP3A4 and ∼58 for CYP3A5 (Table 1).

Substrate Protection. The inactivation of CYP3A4 by FUT was attenuated in a dose-dependent manner by the coincubation of testosterone, an alternative substrate of CYP3A (Fig. 4B). Similarly, the incorporation of the potent CYP3A direct inhibitor ketoconazole at a concentration of 0.1 μM also diminished the rate of inactivation (Fig. 4C). However, unlike with testosterone, enzyme inactivation was abolished when 1 μM ketoconazole was coincubated with FUT and CYP3A4 in the primary incubation mixture, indicating that complete protection against inactivation had taken place. Similarly, these trends in substrate protection were also recapitulated in CYP3A5 (Supplemental Fig. 2, B and C).

Effect of Exogenous Nucleophile and Scavenger of ROS on Inactivation. On the other hand, the inclusion of GSH and catalase did not offer any appreciable protection from inactivation, whereas CYP3A4 and CYP3A5 were inactivated to a similar extent as incubation mixtures comprising FUT alone (Fig. 4D) (Supplemental Fig. 2D).

Reversibility of Inactivation. Dialysis and chemical oxidation with potassium ferricyanide were conducted to delineate the specific nature of inactivation of CYP3A by FUT (i.e., pseudo-irreversible or irreversible). The results of the first series of experiments revealed an absence of CYP3A activity recovery following dialysis at 4°C for 4 hours (Fig. 5A) (Supplemental Fig. 3A). It should be noted that the marginal drop in the remaining enzyme activity observed after dialysis could be explained by enzymatic degradation that occurred during the course of dialysis. In the second series of experiments, potassium ferricyanide only modestly restored the metabolic activity of CYP3A4 and CYP3A5 by 1.3 ± 0.3% and 5.6 ± 1.3%, respectively, after a 30-minute preincubation with 25 μM FUT (Fig. 5B) (Supplemental Fig. 3B), which was grossly under the predefined threshold of 20% for MIC-forming inactivators (Watanabe et al., 2007).

Spectral Difference Scanning. To further substantiate the proposed mechanism of inactivation evoked by FUT against CYP3A, spectral difference scanning was performed. The results of these experiments revealed that the absorbance difference measured in CYP3A4 incubations over a 1-hour duration failed to detect a spectrally resolvable peak in the Soret region (448–458 nm), commonly associated with MIC (Fig. 5C) (Polasek and Miners, 2008). Moreover, tracking the increase in absorbance between 454 nm and the

TABLE 2

Accurate mass measurement of the parent and product ions of FUT-G1 using a mass tolerance cutoff of ≤5 ppm

Proposed Elemental Composition	Theoretical *m/z*	Experimental *m/z*	Mass Accuracy	
			ΔDa	Δppm
$C_{32}H_{40}O_9N_9S$	726.2664	726.2629	−0.0035	−4.8
$C_{32}H_{38}O_8N_9S$	708.2559	708.2528	−0.0031	−4.4
$C_{27}H_{33}O_6N_8S$	597.2238	597.2212	−0.0026	−4.4
$C_{19}H_{21}O_2N_6$	365.1721	365.1704	−0.0017	−4.7

isosbestic point at 490 nm against time further corroborated the lack of MIC formation with FUT (Fig. 5D). These observations were also consistent in parallel experiments conducted with CYP3A5 (Supplemental Fig. 3, C and D).

GSH Trapping. A GSH trapping assay was conducted to profile reactive intermediates that could have perpetrated covalent modification of CYP3A, leading to its inactivation. Here, we adopted the well-established PIS at *m/z* 272 in negative mode and constant NL scan of 129 Da in positive mode, which monitors for the loss of the deprotonated γ-glutamyl-dehydroalanyl-glycine and pyroglutamic acid moiety, respectively, from GSH (Baillie and Davis, 1993; Dieckhaus et al., 2005). Notably, these survey scans evinced two peaks suggestive of FUT-derived GSH adducts; namely FUT-G1 (retention time: 6.32 minutes) and FUT-G2 (retention time: 6.24 minutes) with $[M+H]^+$ ion at *m/z* of 726.1 and 742.3, respectively, that were absent in vehicle-containing samples (Fig. 6, A and D) and only detected in incubation mixtures comprising FUT (Fig. 6, B and E). Intriguingly, we were unable to detect the less abundant FUT-G2 peak when rhCYP3A4 was replaced with potassium phosphate buffer (Fig. 6, C and F). The resultant enhanced product ion MS/MS spectra further reinforced our postulations that both peaks corresponded to GSH adducts due to its characteristic collision-induced dissociation fragmentation pattern, yielding neutral mass loss of 129 Da (corresponding to the loss of a pyroglutamate moiety) (Supplemental Fig. 4, A–D). Accurate mass measurements were then performed to elucidate the structures of FUT-G1 and FUT-G2. As expected, we were able to recapitulate the nominal mass patterns generated using the QTRAP-MS when the GSH conjugates were subjected to accurate mass measurements using the Orbitrap-MS. The proposed elemental composition, theoretical and experimental exact *m/z*, and mass accuracy (in both ΔDa and Δppm) of FUT-G1 and FUT-G2 are outlined in Tables 2 and 3, respectively. Additionally, the representative product ion chromatogram, accurate mass spectrum, and proposed fragmentation pattern of FUT-G1 and FUT-G2 are illustrated in Fig. 7, A–D.

Discussion

FUT is a novel irreversible inhibitor of FGFR1–4 that is currently under clinical investigation for intrahepatic cholangiocarcinoma. Although early studies have reported that FUT inhibits CYP3A in vitro, the exact biochemical nature underpinning its inhibition profile remains obscure. Our study revealed that FUT inactivated CYP3A-mediated rivaroxaban hydroxylation in a manner that is consistent with MBI. Thereafter, using high-resolution mass spectrometry, we discovered that FUT is amenable to metabolic activation at its acrylamide moiety to an unstable epoxide intermediate that is likely implicated in the covalent inactivation of CYP3A.

From a drug discovery standpoint, inactivators that possess a larger k_{inact} and a smaller K_I value generally have a larger propensity to elicit DDI in vivo. Consequently, the k_{inact}/K_I ratio is frequently employed as a metric to quantitatively assess the in vitro inactivation potency of a preclinical drug candidate (Orr et al., 2012). Comparing the k_{inact}/K_I ratios derived for CYP3A4 revealed that the inactivation potency of FUT was in the same order of magnitude as the other FDA-approved FGFR inhibitors (Table 4). Moreover, the apparent k_{obs} for CYP3A4 and CYP3A5 at 10 μM was calculated to be 0.11 $minutes^{-1}$ and 0.01 $minutes^{-1}$, respectively, thereby implying that only the inactivation of CYP3A4 is likely to constitute a potential in vivo pharmacokinetic DDI risk (Zimmerlin et al., 2011). Unfortunately, a more precise estimation of its DDI risk cannot be evaluated at this point, as FUT is still an investigational drug. Consequently, there is a dearth of other relevant drug-dependent parameters in the scientific literature and public domain. Another important parameter of an MBI is its partition ratio, which is widely regarded as a quantitative measure of its inactivation efficiency. While the exact mechanistic basis underscoring the differential efficiencies is contingent on a complex interplay of biochemical factors, such as the intrinsic reactivity of the intermediate formed and the adjacency to its intended substructural target within the enzymatic active site (Nassar et al., 2008), there is broad consensus that inactivators possessing partition ratios under 50 are highly efficient (Lim et al., 2005). Consequently, our findings implied that the inactivation of CYP3A4 by FUT is only moderately efficient and pales in comparison with those obtained for the other three FDA-approved FGFR inhibitors (Table 4). Furthermore, while the coincubation with scavenger nucleophiles (i.e., GSH and catalase) afforded virtually no protection against inactivation, it is starkly contrasted with the incorporation of testosterone or ketoconazole—which markedly attenuated the observed rate of inactivation. These findings shed some light into CYP3A4's molecular determinants by further substantiating that inactivation likely occurred within its active site and thus could be protected by a competing substrate or a

TABLE 3

Accurate mass measurement of the parent and product ions of FUT-G2 using a mass tolerance cutoff of ≤5 ppm

Proposed Elemental Composition	Theoretical *m/z*	Experimental *m/z*	Mass Accuracy	
			ΔDa	Δppm
$C_{32}H_{40}O_{10}N_9S$	742.2613	742.2627	0.0014	1.9
$C_{32}H_{38}O_9N_9S$	724.2508	724.2473	−0.0035	−4.8
$C_{32}H_{36}O_8N_9S$	706.2402	706.2370	−0.0034	−4.8
$C_{27}H_{33}O_7N_8S$	613.2187	613.2159	−0.0028	−4.6
$C_{27}H_{31}O_6N_8S$	595.2082	595.2055	−0.0027	−4.5
$C_{15}H_{14}O_2N_5$	296.1142	296.1127	−0.0015	−5.0

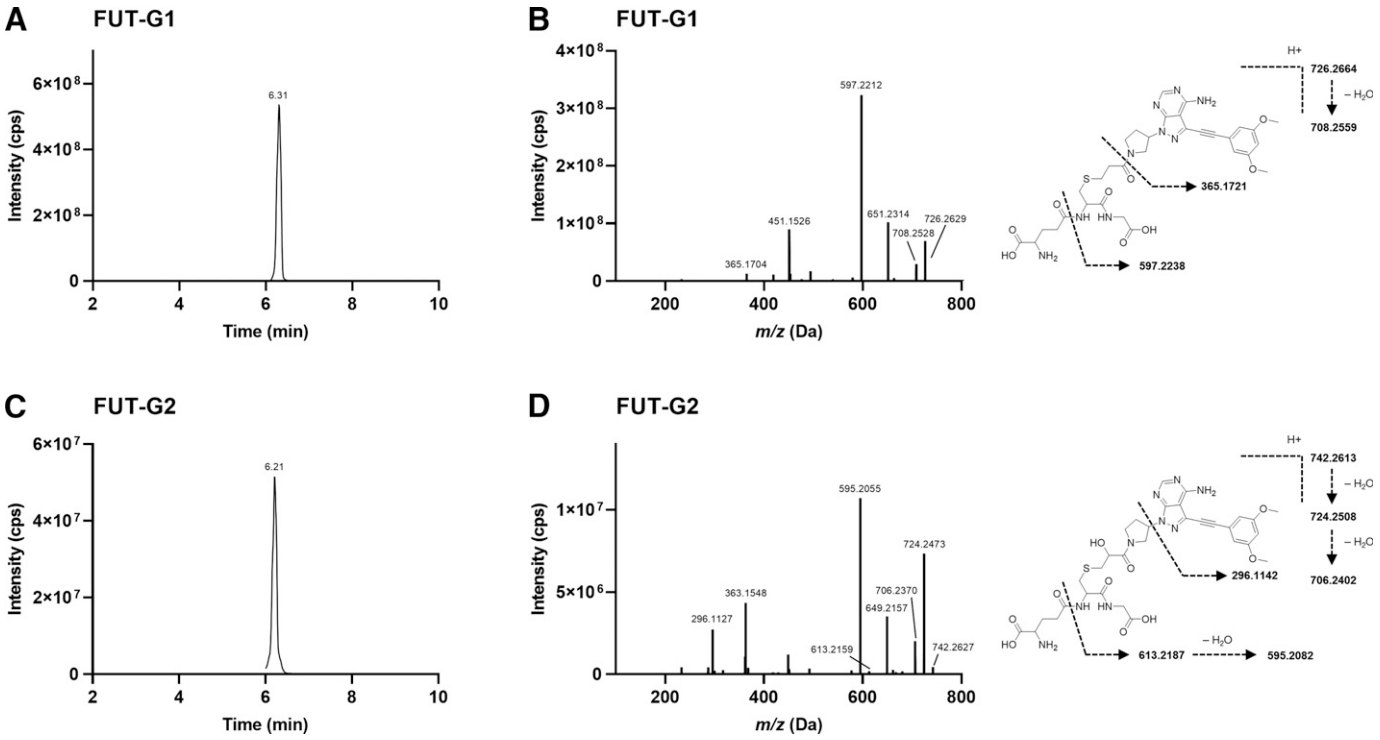

Fig. 7. (A) Representative product ion chromatogram of (A) FUT-G1 and (B) FUT-G2. Proposed accurate mass fragmentation pattern of (C) FUT-G1 and (D) FUT-G2. The exact mass spectra depict the experimental *m/z* values, whereas the chemical structures (inset) illustrate the theoretical accurate *m/z* values of the parent and product ions of the two GSH adducts formed in situ in the GSH trapping assay as outlined in Tables 2 and 3 using a strict mass tolerance cutoff of ≤5 ppm.

potent inhibitor. Importantly, these results also ruled out potentially confounding artifactual causes of inactivation (i.e., production of ROS in the P450 catalytic cycle) and are well-aligned with our earlier postulation that the time-dependent loss of enzymatic activity engendered by FUT stemmed from a putative reactive intermediate that is formed via P450-mediated metabolic activation.

A series of three experiments was then performed to decipher if CYP3A inactivation arose through an MIC or via covalent modification. In broad strokes, MIC results from the chelation of the heme catalytic ferrous iron by the chemically reactive intermediate via a strong coordinate bond. While such coordination complexes are stable in vivo, they may be dissipated under certain in vitro conditions, which allows them to be distinguished experimentally. This is commonly achieved via dialysis or chemical oxidation using potassium ferricyanide to revert the heme iron back to its reduced ferric ground state, and in doing so liberate it from the tight-binding complex with the inactivator and restore its catalytic activity. This explains why MICs are termed as pseudo-irreversible. Conversely, covalent alkylation of the P450 apoprotein and/or prosthetic heme culminates in an irrevocable loss of enzyme activity that cannot be alleviated by either aforementioned methodology. Notably, aniline-based drugs like dapsone and procainamide have previously been reported to be capable of undergoing P450-mediated oxidation to a labile nitroso intermediate that is capable of forming an MIC (Kalgutkar et al., 2007). As FUT similarly possesses an anilyl moiety, it was imperative to interrogate whether it elicited any pseudo-irreversible inactivation of CYP3A. Here, results from all three assays were in concordance and collectively asserted that the nature of inactivation of CYP3A by FUT was unlikely to be pseudo-irreversible, and instead arose from the covalent modification of the P450 apoprotein and/or its heme moiety due to the lack of substantial enzyme activity recovery following dialysis and chemical oxidation, as well as the absence of the diagnostic Soret peak in spectral analyses.

We next sought to establish the identities of the reactive intermediate that could engender covalent modification of CYP3A. This was achieved by fortifying the reaction mixtures with saturating amounts of GSH, which serves to readily trap the labile reactive species generated in situ as stable conjugates and facilitate their eventual detection via the application of two complementary UPLC-MS/MS survey scans based on known GSH fragmentation patterns. These survey scans subsequently triggered the acquisition of two prospective GSH adducts (i.e., FUT-G1 and FUT-G2) that eluted very closely together, which seemed to imply that they were structurally similar. However, as FUT

TABLE 4

Comparison of the CYP3A4 enzyme inactivation kinetic parameters between FUT and the other FDA-approved FGFR inhibitors using morpholinone hydroxylation of rivaroxaban as an in vitro marker reaction of residual CYP3A activity

Compound	K_I (μM)	k_{inact} (min^{-1})	k_{inact}/K_I (min^{-1} mM^{-1})	Partition Ratio	Reference
FUT	12.5	0.25	20.0	52	
Erdafitinib	4.0	0.12	30.0	32	(Tang et al., 2021a)
Infigratinib	4.2	0.07	16.7	41	(Tang et al., 2021b)
Pemigatinib	8.7	0.11	12.6	44	(Tang et al., 2022)

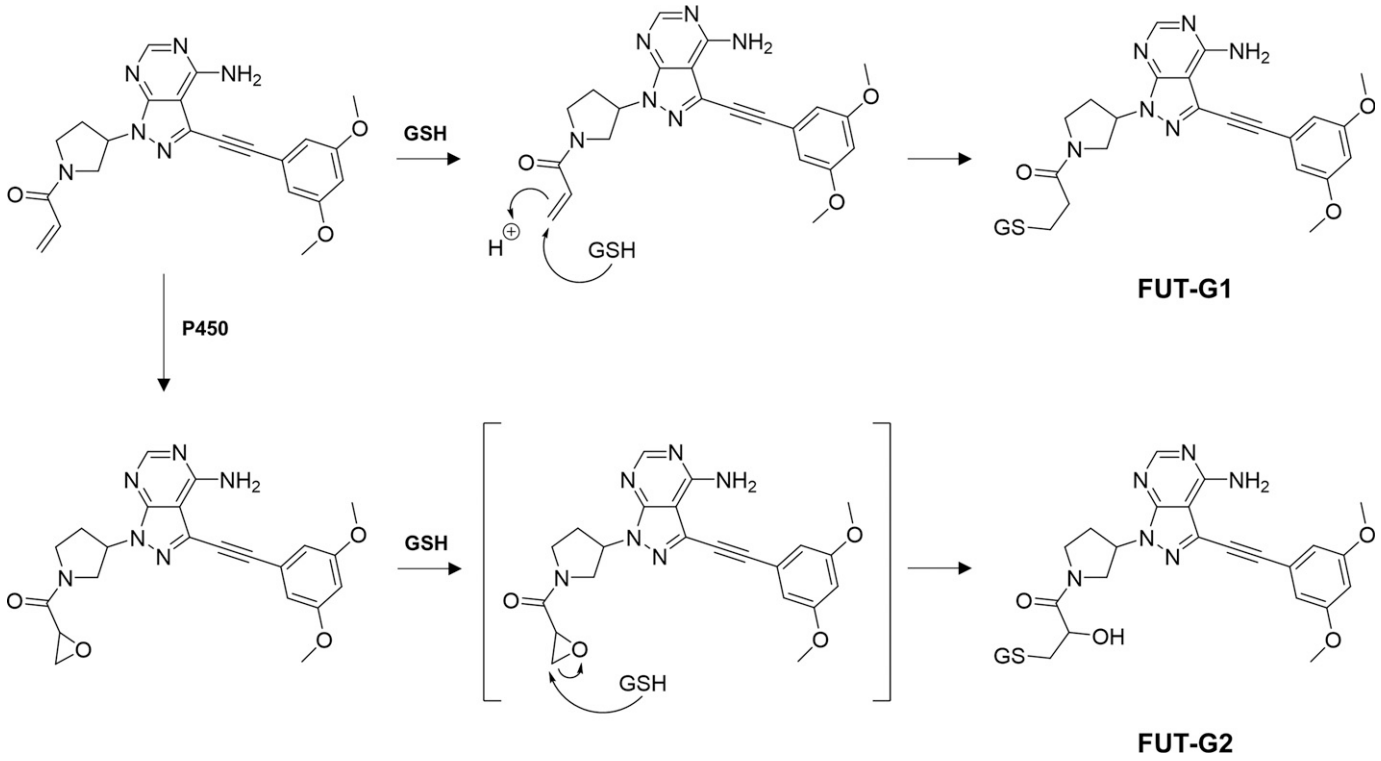

Fig. 8. Proposed chemical pathway for the formation of the GSH conjugates FUT-G1 and FUT-G2. FUT-G1 is formed by the nonenzymatic conjugation of GSH to FUT via Michael addition whereas FUT-G2 is formed via the nucleophilic attack of GSH to an epoxide intermediate generated from P450-mediated metabolic activation of FUT at its acrylamide electrophilic warhead.

contains an electrophilic acrylamide warhead that is known to be capable of directly conjugating to GSH via Michael addition (Schwöbel et al., 2010), we were curious whether the GSH adducts profiled earlier arose directly from FUT or indirectly through a reactive intermediate formed via metabolic activation of the parent compound. Strikingly, we demonstrated that when rhCYP3A4 was substituted with potassium phosphate buffer it resulted in the loss of the less abundant peak, which corresponded to FUT-G2. This suggested that P450-mediated metabolic activation was a crucial step that culminated in the formation of FUT-G2. Our conjectures were proven to be correct in our high-resolution Orbitrap-MS analysis using a strict mass tolerance threshold of 5 ppm, which enabled us to confidently establish that FUT-G1 was formed by the nonenzymatic conjugation of GSH to FUT via Michael addition, whereas FUT-G2 resulted from an epoxide intermediate generated from P450-mediated metabolic activation of FUT at its acrylamide electrophilic warhead (Fig. 8). Notably, the formation of FUT-G1 via direct GSH conjugation is similarly observed for other acrylamide-containing drugs and may play a significant role in its extrahepatic clearance although further pharmacokinetic studies are needed to evaluate its actual contribution (Shibata and Chiba, 2015). On the other hand, the formation of FUT-G2 is substantiated by a previous study which reported the in vivo P450-mediated epoxidation of acrylamide (Ghanayem et al., 2005). Importantly, as we previously demonstrated that NADPH cofactor was necessary for FUT to evoke enzymatic inactivation, we believe that this epoxide metabolite was likely responsible for the covalent modification of the CYP3A. However, as our experiments did not yield direct evidence of covalent binding, future work involving MS-based proteomics methodologies are necessary to validate our postulations.

Targeted covalent inhibitors like FUT represent an emerging subcategory of tyrosine kinase inhibitors that typically possess an α,β-unsaturated carbonyl scaffold (i.e., acrylamide moiety), which allows it to covalently bind to a cysteine residue after the molecule is tightly held in place within the active site by noncovalent interactions. This modality confers several attractive pharmacological advantages over conventional reversible ATP-competitive inhibitors, such as an increased biochemical potency, a sustained duration of action, and the potential to circumvent resistance arising through gatekeeper mutations (Carmi et al., 2012; Kalgutkar and Dalvie, 2012). Although such drugs present a potential toxicological concern arising from aberrant off-target covalent protein modification, this risk is mitigated by the low intrinsic electrophilicity of the acrylamide moiety, which ensures that the covalent interaction can only ensue if the molecule is tightly positioned within the binding pocket of its desired biologic target. At present, several FDA-approved covalent inhibitors with acrylamide warheads (i.e., ibrutinib, osimertinib) are routinely used in the clinical setting and have demonstrated reasonable safety profiles. However, our study demonstrates that the acrylamide scaffold in targeted covalent inhibitors is amenable to being metabolically activated to a highly reactive epoxide intermediate. Due to their inherent ring strain, epoxides possess a greater electrophilic burden and can directly interact with DNA or cellular proteins to form adducts that may potentially induce mutagenicity and cytotoxicity (Ghanayem et al., 2005). Although there are no current reports of idiosyncratic toxicities with FUT, our findings may serve as a premonitory indicator of reactive metabolite-induced toxicity. More importantly, as the relative abundance of these epoxide-derived GSH adducts (i.e., FUT-G2) tend to be eclipsed by those formed nonenzymatically (i.e., FUT-G1), it could masquerade as a single combined peak in UPLC-MS/MS survey scans and evade detection. Consequently, we advocate for closer scrutiny to be adopted when profiling the reactive metabolites of compounds possessing an α,β-unsaturated carbonyl scaffold.

In conclusion, we established that FUT is a typical MBI of CYP3A. Furthermore, using FUT as an exemplary targeted covalent inhibitor, our study reveals the propensity for its acrylamide Michael acceptor to be metabolically activated to an epoxide, which likely engendered covalent inactivation of CYP3A. The findings reported in this study are clinically relevant due to the growing resurgence of therapeutic covalent inhibitors.

Authorship Contributions

Participated in research design: Tang, Chan.
Conducted experiments: Tang, Fu, Koh, Wu.
Contributed new reagents or analytic tools: Zhou.
Performed data analysis: Tang, Fu, Wu.
Wrote or contributed to the writing of the manuscript: Tang, Chan.

References

Baillie TA and Davis MR (1993) Mass spectrometry in the analysis of glutathione conjugates. *Biol Mass Spectrom* **22**:319–325.

Bjornsson TD, Callaghan JT, Einolf HJ, Fischer V, Gan L, Grimm S, Kao J, King SP, Miwa G, Ni L, et al.; Pharmaceutical Research and Manufacturers of America (PhRMA) Drug Metabolism/Clinical Pharmacology Technical Working Group; FDA Center for Drug Evaluation and Research (CDER) (2003) The conduct of in vitro and in vivo drug-drug interaction studies: a Pharmaceutical Research and Manufacturers of America (PhRMA) perspective. *Drug Metab Dispos* **31**:815–832.

Carmi C, Mor M, Petronini PG, and Alfieri RR (2012) Clinical perspectives for irreversible tyrosine kinase inhibitors in cancer. *Biochem Pharmacol* **84**:1388–1399.

Chakrabarti S, Finnes HD, and Mahipal A (2022) Fibroblast growth factor receptor (FGFR) inhibitors in cholangiocarcinoma: current status, insight on resistance mechanisms and toxicity management. *Expert Opin Drug Metabl Toxicol* **18**:85–98.

Dieckhaus CM, Fernández-Metzler CL, King R, Krolikowski PH, and Baillie TA (2005) Negative ion tandem mass spectrometry for the detection of glutathione conjugates. *Chem Res Toxicol* **18**:630–638.

Ghanayem BI, McDaniel LP, Churchwell MI, Twaddle NC, Snyder R, Fennell TR, and Doerge DR (2005) Role of CYP2E1 in the epoxidation of acrylamide to glycidamide and formation of DNA and hemoglobin adducts. *Toxicol Sci* **88**:311–318.

Goyal L, Meric-Bernstam F, Hollebecque A, Valle JW, Morizane C, Karasic TB, Abrams TA, Furuse J, He Y, Soni N, Benhadji KA, and Bridgewater JA (2020) FOENIX-CCA2: A phase II, open-label, multicenter study of futibatinib in patients (pts) with intrahepatic cholangiocarcinoma (iCCA) harboring FGFR2 gene fusions or other rearrangements. *Journal of Clinical Oncology* **38**:108.

Guengerich FP (2001) Common and uncommon cytochrome P450 reactions related to metabolism and chemical toxicity. *Chem Res Toxicol* **14**:611–650.

Guengerich FP (2011) Mechanisms of drug toxicity and relevance to pharmaceutical development. *Drug Metab Pharmacokinet* **26**:3–14.

Helsten T, Elkin S, Arthur E, Tomson BN, Carter J, and Kurzrock R (2016) The FGFR Landscape in Cancer: Analysis of 4,853 Tumors by Next-Generation Sequencing. *Clin Cancer Res* **22**:259–267.

Ho HK, Chan JCY, Hardy KD, and Chan ECY (2015) Mechanism-based inactivation of CYP450 enzymes: a case study of lapatinib. *Drug Metab Rev* **47**:21–28.

Kalgutkar AS and Dalvie DK(2012) Drug discovery for a new generation of covalent drugs. *Expert Opin Drug Discov* **7**:561–581.

Kalgutkar AS, Obach RS, and Maurer TS (2007) Mechanism-based inactivation of cytochrome P450 enzymes: chemical mechanisms, structure-activity relationships and relationship to clinical drug-drug interactions and idiosyncratic adverse drug reactions. *Curr Drug Metab* **8**:407–447.

Kitz R and Wilson IB (1962) Esters of methanesulfonic acid as irreversible inhibitors of acetylcholinesterase. *J Biol Chem* **237**:3245–3249.

Lim HK, Duczak Jr N, Brougham L, Elliot M, Patel K, and Chan K (2005) Automated screening with confirmation of mechanism-based inactivation of CYP3A4, CYP2C9, CYP2C19, CYP2D6, and CYP1A2 in pooled human liver microsomes. *Drug Metab Dispos* **33**:1211–1219.

Masubuchi Y and Horie T (2007) Toxicological significance of mechanism-based inactivation of cytochrome P450 enzymes by drugs. *Crit Rev Toxicol* **5**:389–412.

Nassar AF, Hollenberg PF, and Scatina J (2008) *Drug Metabolism Handbook: Concepts and Applications,* WileyCity, Chichester, UK.

Orr STM, Ripp SL, Ballard TE, Henderson JL, Scott DO, Obach RS, Sun H, and Kalgutkar AS (2012) Mechanism-based inactivation (MBI) of cytochrome P450 enzymes: structure-activity relationships and discovery strategies to mitigate drug-drug interaction risks. *J Med Chem* **55**:4896–4933.

Polasek TM and Miners JO (2008) Time-dependent inhibition of human drug metabolizing cytochromes P450 by tricyclic antidepressants. *Br J Clin Pharmacol* **65**:87–97.

Porta R, Borea R, Coelho A, Khan S, Araújo A, Reclusa P, Franchina T, Van Der Steen N, Van Dam P, Ferri J, et al. (2017) FGFR a promising druggable target in cancer: Molecular biology and new drugs. *Crit Rev Oncol Hematol* **113**:256–267.

Schwöbel JAH, Wondrousch D, Koleva YK, Madden JC, Cronin MTD, and Schüürmann G (2010) Prediction of michael-type acceptor reactivity toward glutathione. *Chem Res Toxicol* **23**:1576–1585.

Shibata Y and Chiba M (2015) The role of extrahepatic metabolism in the pharmacokinetics of the targeted covalent inhibitors afatinib, ibrutinib, and neratinib. *Drug Metab Dispos* **43**:375–384.

Silverman RB (1995) Mechanism-based enzyme inactivators. *Methods Enzymol* **249**:240–283.

Sootome H, Fujita H, Ito K, Ochiiwa H, Fujioka Y, Ito K, Miura A, Sagara T, Ito S, Ohsawa H, et al. (2020) Futibatinib Is a Novel Irreversible FGFR 1-4 Inhibitor That Shows Selective Antitumor Activity against FGFR-Deregulated Tumors. *Cancer Res* **80**:4986–4997.

Tang LWT and Chan ECY (2022) Quantification of the irreversible fibroblast growth factor receptor inhibitor futibatinib by UPLC-MS/MS: Application to the metabolic stability assay in human liver microsomes for the estimation of its in vitro hepatic intrinsic clearance. *J Pharm Biomed Anal* **214**:114731.

Tang LWT, Teng JW, Koh SK, Zhou L, Go ML, and Chan ECY (2021a) Mechanism-Based Inactivation of Cytochrome P450 3A4 and 3A5 by the Fibroblast Growth Factor Receptor Inhibitor Erdafitinib. *Chem Res Toxicol* **34**:1800–1813.

Tang LWT, Teng JW, Verma RK, Koh SK, Zhou L, Go ML, Fan H, and Chan ECY (2021b) Infigratinib Is a Reversible Inhibitor and Mechanism-Based Inactivator of Cytochrome P450 3A4. *Drug Metab Dispos* **49**:856–868.

Tang LWT, Verma RK, Fan H, and Chan ECY (2021c) Mechanism-Based Inactivation of Cytochrome P450 3A4 by Benzbromarone. *Mol Pharmacol* **99**:266–276.

Tang LWT, Wei W, Verma RK, Koh SK, Zhou L, Fan H, and Chan ECY (2022) Direct and Sequential Bioactivation of Pemigatinib to Reactive Iminium Ion Intermediates Culminate in Mechanism-Based Inactivation of Cytochrome P450 3A. *Drug Metab Dispos* **50**:529–540.

Touat M, Ileana E, Postel-Vinay S, André F, and Soria JC (2015) Targeting FGFR signaling in cancer. *Clin Cancer Res* **21**:2684–2694.

Watanabe A, Nakamura K, Okudaira N, Okazaki O, and Sudo K (2007) Risk assessment for drug-drug interaction caused by metabolism-based inhibition of CYP3A using automated in vitro assay systems and its application in the early drug discovery process. *Drug Metab Dispos* **35**:1232–1238.

Yamamiya I, Laabs J, Hunt A, Takenaka T, Sonnichsen D, Mina M, He Y, and Benhadji K (2021) Abstract CT125: Evaluation of potential drug-drug interactions (DDIs) between futibatinib and CYP3A inhibitors/inducers, CYP3A substrates, or proton pump inhibitors (PPIs). *Cancer Res* **81**:CT125–CT125.

Zanger UM, Turpeinen M, Klein K, and Schwab M (2008) Functional pharmacogenetics/genomics of human cytochromes P450 involved in drug biotransformation. *Anal Bioanal Chem* **392**:1093–1108.

Zimmerlin A, Trunzer M, and Faller B (2011) CYP3A time-dependent inhibition risk assessment validated with 400 reference drugs. *Drug Metab Dispos* **39**:1039–1046.

Address correspondence to: Eric Chun Yong Chan, Department of Pharmacy, National University of Singapore, 18 Science Drive 4, Singapore 117543. E-mail: phaccye@nus.edu.sg

Supplemental Data

Metabolic Activation of the Acrylamide Michael Acceptor Warhead in Futibatinib to an Epoxide Intermediate Engenders Covalent Inactivation of Cytochrome P450 3A

Lloyd Wei Tat Tang[1], Jiaxin Fu[1], Siew Kwan Koh[2], Guoyi Wu[1], Lei Zhou[2,3,4] and Eric Chun Yong Chan[1]

[1]Department of Pharmacy, Faculty of Science, National University of Singapore, Singapore

[2]Singapore Eye Research Institute (SERI), Singapore

[3]Department of Ophthalmology, Yong Loo Lin School of Medicine, National University of Singapore, Singapore

[4]Ophthalmology and Visual Sciences Academia Clinical Program, Duke-National University of Singapore Medical School, Singapore

SUPPLEMENTAL METHODS

Measurement of Hydroxylated Rivaroxaban (CYP3A Activity) by UPLC-MS/MS. All samples described in this work were analysed using the UPLC-MS/MS system consisting of an Agilent 1290 Infinity ultra-high pressure liquid chromatography system (Agilent Technologies Inc., Santa Clara, CA) interfaced with a triple quadrupole mass spectrometer (AB SCIEX Triple Quad 3500 MS system equipped with a Turbo V ion source; AB SCIEX, Framingham, MA). Chromatographic separation was achieved with an ACQUITY UPLC ethylene bridged hybrid C_{18}, 2.2 × 100 mm, 1.7 µM column (Waters, Milford, MA). The aqueous mobile phase (A) was 0.1% formic acid in water, whereas the organic mobile phase (B) was 0.1% formic acid in acetonitrile. Mobile phases were delivered at a flow rate of 0.5 mL/min. The column and sample temperature were thermostated at 45°C and 4°C respectively. The gradient elution conditions were as follows: linear gradient from 20 to 80% B (0 – 1.20 min), isocratic at 100% B (1.21 – 2.00 min) and isocratic at 20% B (2.01 – 2.50 min). All analytes were detected in positive electrospray ionization (ESI) mode. The source-dependent MS parameters were as follows: ion spray voltage = 5500 V; source temperature = 550°C; curtain gas (CUR) = 20 psi; ion source gas 1 (sheath gas) = 40 psi; ion source gas 2 (drying gas) = 45 psi. The MRM transitions and compound-dependent MS parameters of hydroxylated rivaroxaban and dexamethasone (internal standard) are summarized in **Supplemental Table 1**. Chromatographic peak integration was performed using MultiQuant software version 3.0 (Applied Biosystems, Foster City, CA). For all UPLC-MS/MS analyses, the peak area of the analyte was expressed as a ratio to the peak area of the internal standard.

Supplemental Fig. 1. (A) Time- and concentration-dependent inactivation of CYP3A5-mediated rivaroxaban hydroxylation by FUT. (B) Nonlinear least square regression of k_{obs} versus various concentrations of FUT yielded K_I and k_{inact} values of 51.4 ± 21.4 μM and 0.06 ± 0.02 min^{-1}. (C) Inactivation of CYP3A5 by FUT also exhibited cofactor-dependency. Each point in (A to C) represents the mean and S.D. of triplicate experiments.

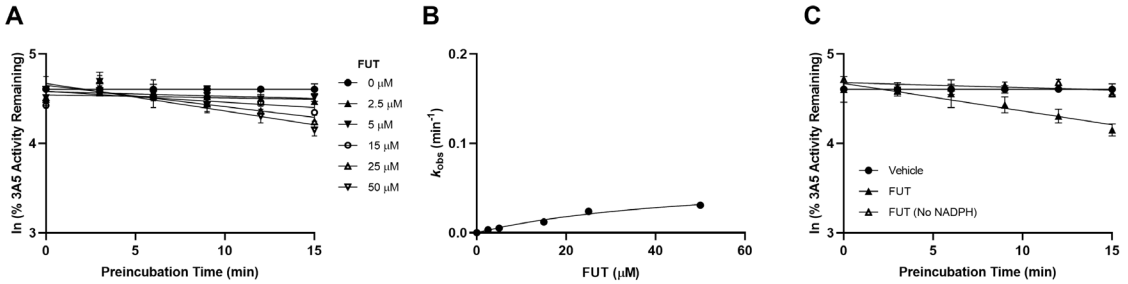

Supplemental Fig. 2. (A) Partition ratio for the inactivation of CYP3A5 by FUT was estimated to be 58. Inactivation of CYP3A5 was diminished by coincubation with (B) an alterative CYP3A substrate (testosterone) and considerably abrogated by (C) a direct inhibitor of CYP3A (ketoconazole). (D) On the other hand, the inclusion of either an exogenous nucleophile (GSH) or a scavenger of ROS (catalase) did not confer substrate protection. Each point in (A to D) represents the mean and S.D. of triplicate experiments.

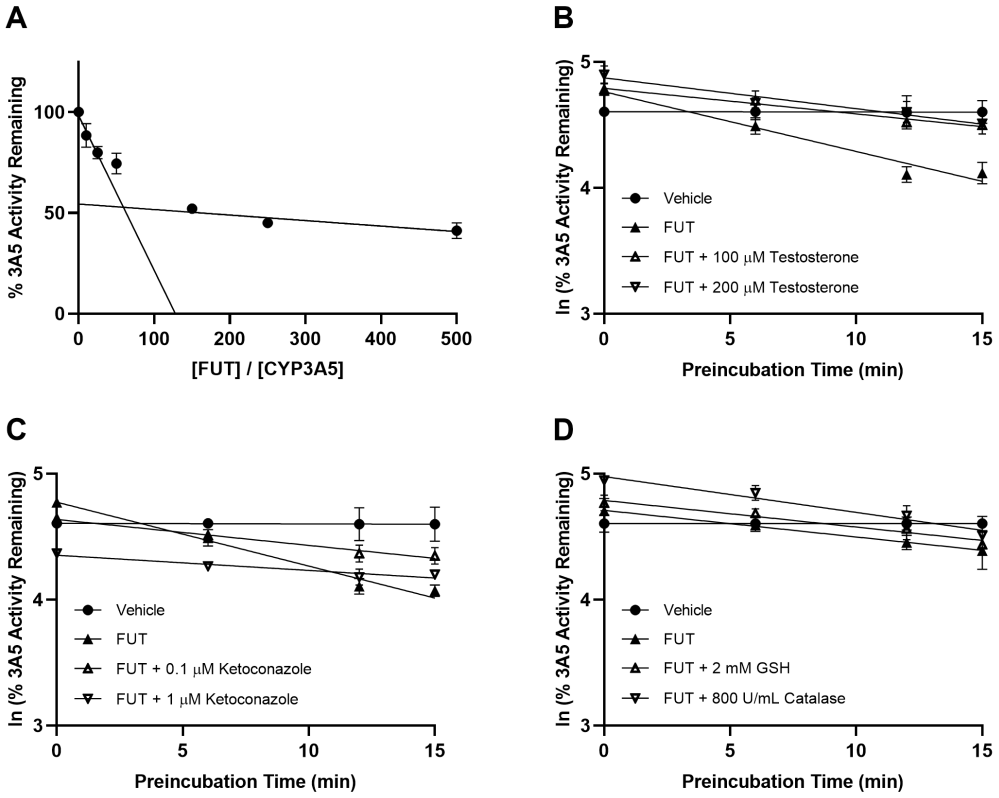

Supplemental Fig. 3. Metabolic activity of CYP3A5 was (A) not restored after extensive dialysis at 4°C for 4 h and (B) only modestly restored by 5.6 ± 1.3% following treatment with 2 mM potassium ferricyanide (KFC). (C) Absorbance difference measured over 1 h failed to detect a spectrally resolvable peak in the Soret region (448 – 458 nm) for CYP3A5 incubated with FUT. (D) Likewise, a comparison of the absorbance at the reference of 454 nm against the isosbestic point at 490 nm failed to demonstrate an increase in the extent of MIC formation over time. Results from (A and B) depict the mean and S.D. of three independent experiments conducted in triplicates.

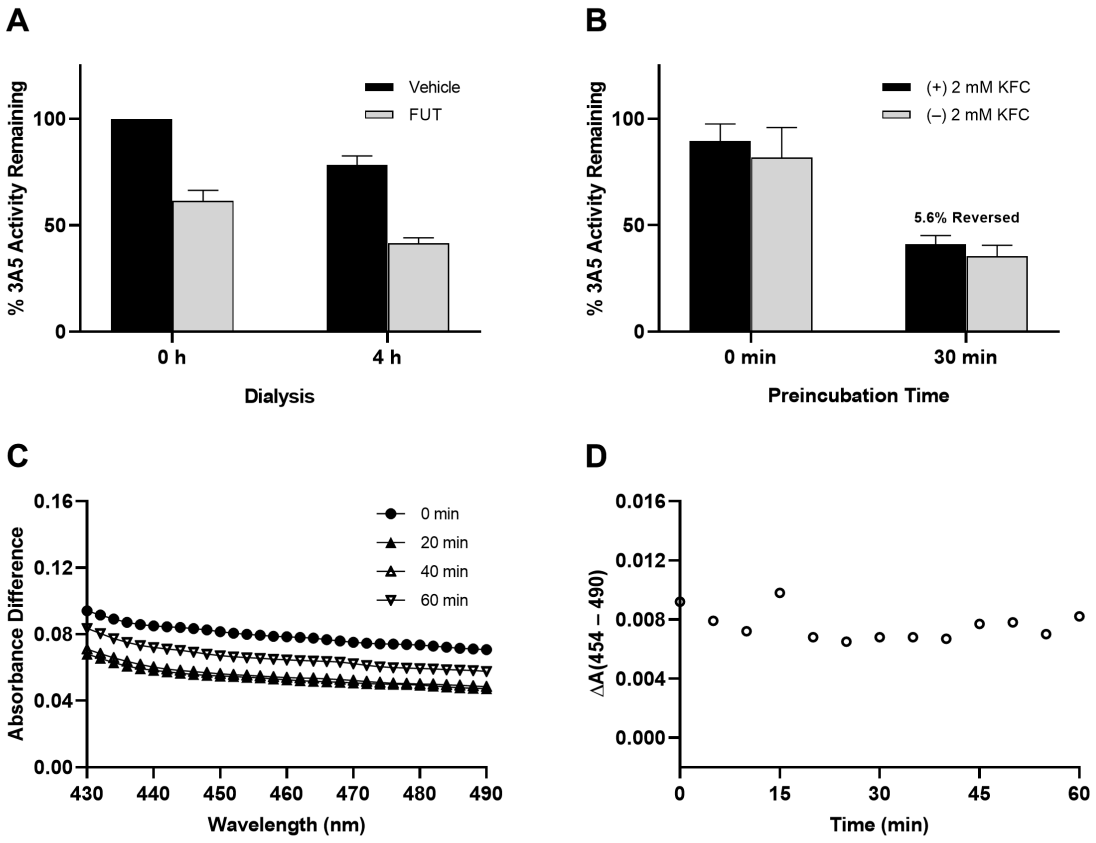

Supplemental Fig. 4. (A) Representative product ion chromatogram of FUT-G1 (retention time: 6.32 min) and its (B) corresponding EPI MS/MS spectra (*m/z* 726.1) and the (C) representative product ion chromatogram of FUT-G2 (retention time: 6.24 min) and its (D) corresponding EPI MS/MS spectra (*m/z* 742.3) formed *in situ* in the GSH trapping assay.

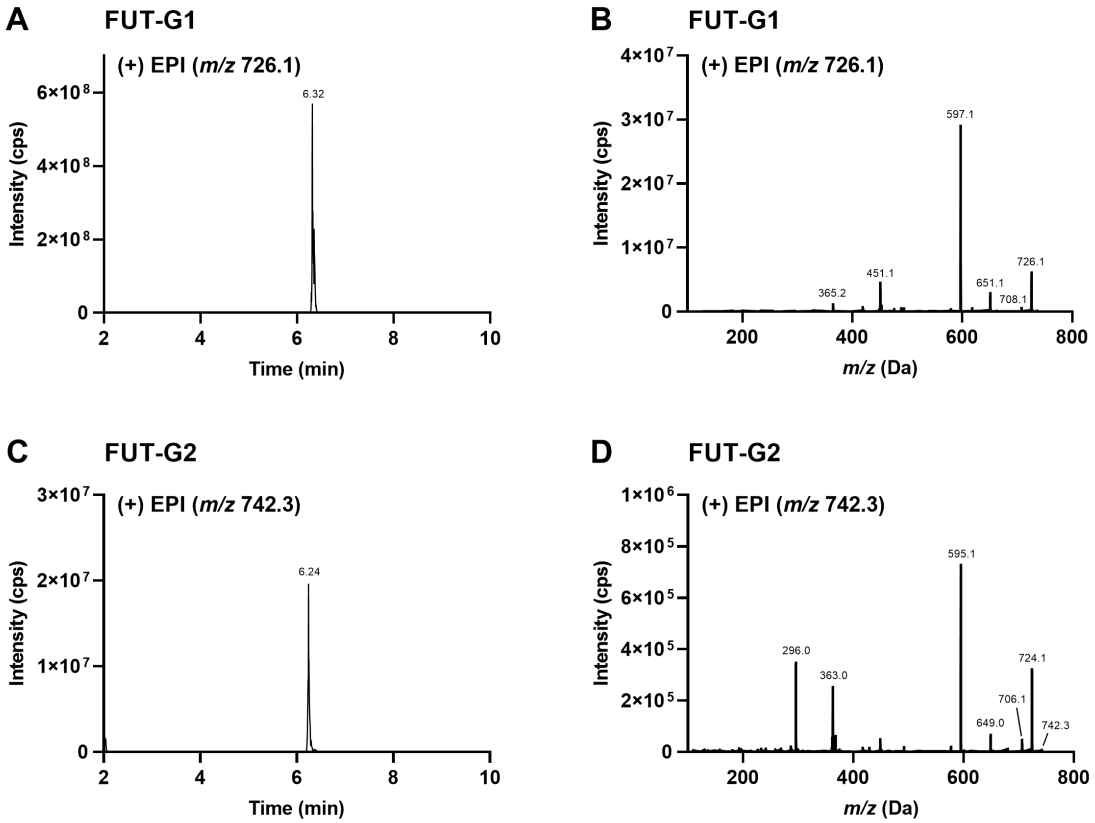

Supplemental Table 1. Optimized compound-dependent MS parameters for UPLC-MS/MS analysis

Compound	Q1 Mass (*m/z*)	Q3 Mass (*m/z*)	DP (V)	EP (V)	CE (V)	CXP (V)
Hydroxylated Rivaroxaban	452	406	90	10	25	9
Dexamethasone	393	355	112	10	14	14

DP: declustering potential, EP: entrance potential, CE: collision energy, CXP: collision exit potential